Mechanically robust, electrically stable metal arrays on plasma-oxidized polydimethylsiloxane for stretchable technologies

Rian Seghir, S. Arscott

Journal of Applied Physics

Mechanically robust, electrically stable metal arrays on plasma-oxidized polydimethylsiloxane for stretchable technologies

Cite as: J. Appl. Phys. **118**, 045309 (2015); https://doi.org/10.1063/1.4927616
Submitted: 12 June 2015 • Accepted: 18 July 2015 • Published Online: 31 July 2015

Rian Seghir and Steve Arscott

Mechanically robust, electrically stable metal arrays on plasma-oxidized polydimethylsiloxane for stretchable technologies

Rian Seghir[a] and Steve Arscott[b]
Institut d'Electronique, de Microélectronique et de Nanotechnologie (IEMN), CNRS UMR8520, University of Lille, Avenue Poincaré, Cité Scientifique, Villeneuve d'Ascq 59652, France

(Received 12 June 2015; accepted 18 July 2015; published online 31 July 2015)

Certain applications of evolving flexible technologies demand that metallic features remain both mechanically robust (crack-free) and electrically stable for large macroscopic mechanical deformation. Examples of this are flexible radio frequency transmission line technologies and soft metamaterials where electromagnetic properties (e.g., functionality and losses), which rely on the integrity of metallic features, are highly sensitive to shape and resistance variation. In this context, we demonstrate here the ability to deposit crack-free chromium/gold metallized mesa structures on polydimethylsiloxane (PDMS) substrates using thermal evaporation. In order to achieve this, the PDMS is exposed to an optimized oxygen plasma prior to the metallization. A shadow mask allowed us to define specific arrays of metallic mesa features having different sizes (100–600 μm) and surface filling factors on plasma-treated and non-treated PDMS. In contrast to non-treated PDMS, we demonstrate for a loading strain $>45\%$ that the local metal mesa strain is $<2\%$ (crack-free) and the electrical resistance variation is <2 for plasma-treated substrates. Such a result is achieved by tailoring the filling factor and the equivalent stiffness ratio of the layers. The relationship between the filling factor, the equivalent stiffness ratio, and the local strain reduction is analytically modelled. This allows one to understand the role of the key parameters in the behavior of the overall flexible system and, in principle, to design optimized systems such as those mentioned above. © *2015 AIP Publishing LLC*. [http://dx.doi.org/10.1063/1.4927616]

I. INTRODUCTION

During the last fifteen years, the design of high performance flexible electronic systems, along with the development of their associated fabrication processes have become very active areas of research both in academia and industry.[1] Despite this, the realization of electronics with performances equivalent to classical technologies using rigid semiconductor wafers still remain a very open problem. First, no overall consensus yet exists regarding the *fundamental fabrication approach* for such stretchable electronics: (1) physically transferring established technology from a rigid wafer to a soft one introduces the problem of wafer removal and bonding onto a flexible substrate, e.g., dry or wet transfer printing[2–4] and (2) depositing thin films (e.g., metals) directly onto soft materials results in the introduction of significant constraints on the entire process due to the mismatch between thermomechanical properties of deposited thin films and flexible host substrates, e.g., metallization-induced residual stresses and cracking. Second, no overall consensus yet exists on the optimized *architecture and materials* of stretchable structures which maintain performances at high and cyclic mechanical strains: (1) the use of deposited rigid conductor materials with complex pattern designs, e.g., wrinkles, serpentine[5] decreasing the in-plane mechanical strain by allowing out-of-plane mechanical strain relaxation;[6–8] (2) the use of a complex substrate design forcing some regions not to deform;[9–12] (3) the use microfluidics and liquid metals;[8,13] or finally (4) the use of conducting polymers.[14]

To illustrate the above challenges, we can take the specific example of high performance applications such as *inter alia* high frequency systems (GHz-THz), transmission lines, and metamaterials.[15–17] In the latter system, the advantage of stretchability is obvious, especially in reconfigurable metamaterials,[18] i.e., tunable optical materials,[19,20] flexible plasmonics,[21] and strain sensing.[22] In terms of fabrication, such systems involve a multi-layer approach with a high density metallization. It seems evident that lithographic approach, rather than a transfer approach, is appropriate to achieve the required system complexity. In addition, the tunability of these systems is brought about by external stress changes whilst at the same time the mechanical integrity of the metallization and the surrounding matrix must be conserved. A critical point here is that one must be able to design such structures not only electromagnetically but also *mechanically*. For example, one requires mechanical models which finely predict changes in metallic mesa dimension, inter-mesa dimension, and changes in the global symmetry of the system. It should be noted that such systems will be subjected to both large and cyclic strains. Thus, it is crucial to avoid fatigue related damage by ensuring that the local metallic mesa strain remains elastic. The objective of the current manuscript is precisely this—by choosing a lithographic/thin film deposition route to avoid the metal film being in the non-elastic domain by providing an optimized fabrication process, design, and parametric modeling.

In principle and according to basic elastic modeling (see Section III and Fig. 1), small and stiff metallized mesa

[a]rian.seghir@iemn.univ-lille1.fr
[b]steve.arscott@iemn.univ-lille1.fr

structures (m) perfectly bonded onto an infinite soft substrate (s) deform significantly less than the substrate (due to their relatively high *equivalent rigidity* compared to the flexible substrate, e.g., *thickness* × *width* × *stiffness*). In theory, this implies both a great stretchability of inter-mesa substrate material and a high mechanical and electrical stability of mesa structures, e.g., Ref. 23. In practice, however, achieving such an idealized mesa feature metallization directly on very soft substrate, e.g., polydimethylsiloxane (PDMS), using sputtering or thermal evaporation techniques, is not trivial. Indeed, two objectives seem conflicting—(1) a high adhesion (good thin film bonding) and (2) low residual tensile stresses (crack-free deposited mesa features). One way of solving this is by pre-stretching the PDMS during metallization to compensate the residual tensile stress incurred during thin film deposition on this material,[24] although such technique are technically cumbersome and not obviously compatible with multi-step processes.

Here, we propose to use an optimized PDMS surface treatment combined with specific feature dimension and metallization density in order to produce micrometric metal features which are flat, crack-free, and electrically stable under high macroscopic mechanical strain loadings. This latter point implies that the metal mesa remains in the elastic regime for high external mechanical loading. Section II presents the sample fabrication—with and without optimized surface oxygen plasma treatment of 10:1 (w:w) PDMS and the electromechanical test set-up. Section III presents the mechanical modeling of PDMS pixelated by metal Cr/Au mesa array. Section IV presents the electromechanical behavior of metal mesas subjected to high strain loading and a comparison with the mechanical modeling. Finally, Section V presents the conclusions of the study.

II. SAMPLE FABRICATION AND ELECTROMECHANICAL TEST SETUP

All processing was performed in a class ISO 5/7 cleanroom. Sylgard® 184 PDMS (Dow Corning Corporation, USA) was purchased as a two component kit—we define the A:B PDMS mixtures with A as the vinyl-terminated base and B as the cross-linker agent (curing agent—CA) weight content, respectively. PDMS samples were prepared by mixing the base and the curing agent at 10:1 (9.1% CA) to obtain a substrate rigidity (elastic modulus) of 2 MPa (Ref. 25) (reference PDMS[26]). Although the authors have recently demonstrated that the rigidity of the host substrate can be boosted, if necessary, by preparing an optimized PDMS/SU-8 mixture.[12] The mixture was then carefully poured into Petri dish and degassed (5 pumping cycles in a vacuum chamber ≈100 mTorr). The prepared PDMS mixture was then placed onto a leveled hotplate for 2 h at 100 °C. Finally, PDMS films where diced to produce 26 mm × 16 mm × 1 mm tensile test samples with a gauge section of about 10 mm × 10 mm (see Fig. 1).

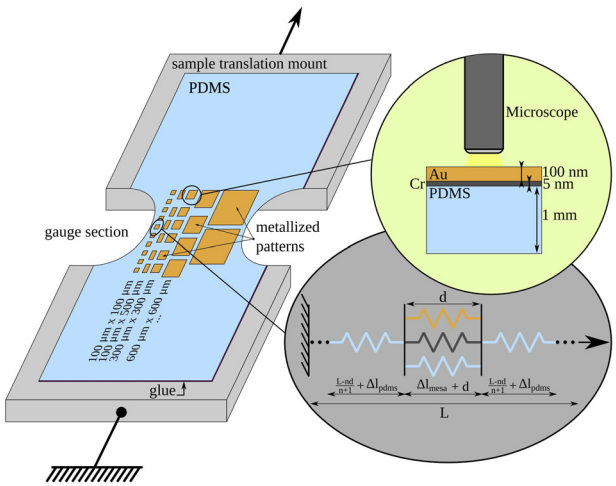

FIG. 1. Schematic diagram of experimental setup and test sample, i.e., a 1 mm thick metallized (Cr/Au—5 nm/100 nm) PDMS film bonded onto an in-house fabricated sample stretcher as well as fully elastic modeling of Cr/Au parallel layers in series on PDMS substrate.

Based on our previous work,[27] some PDMS samples were then treated in a radio frequency (RF) oxygen plasma chamber (Pico-RF, Diener Electronic, Germany) for 30 s/50 W (1.5 kJ) at a chamber pressure of 300 mTorr. The choice of these plasma conditions is crucial and is based on an optimization study,[27] which showed first that a high plasma dose, i.e., >1.8 kJ at 300 mTorr, leads to the formation of an undesirable spontaneous cracking of the silica-like crust formed during the plasma. In contrast, a low plasma dose, i.e., <1 kJ, leads to low surface energy (hydrophobic), which can result in bad adhesion of the metal. The extreme case of this is the non-exposed PDMS—see Fig. 4(a). Thus, an optimized plasma dose appears to be 1.5 kJ—see Fig. 4(b)—which was also observed to be near to the most stable hydrophilic surface as a function of time.[27] In terms of device processing, this last point is important to ensure the chemical stability of the plasma-exposed PDMS surface up to the metallization step. According to the literature, this specific oxygen plasma exposure of PDMS leads to the formation of a ≈15 nm (Refs. 28 and 29) (certainly less than 40 nm, Ref. 30), high surface energy (high bonding), and more brittle (Elastic modulus ≈ 100 MPa, Ref. 31—but crack-free) silica-like crust.

In order to complete the samples, i.e., obtaining 100 nm thick gold arrays bonded onto PDMS, a chromium/gold bilayer is deposited onto the PDMS samples using thermal evaporation. A chromium adhesion layer is used to bond the gold to the PDMS as it is known that gold has poor adhesion to a PDMS surface.[32] Concerning the specific thickness of the chromium, as is the case with optimized oxygen plasma treatment conditions, the chosen chromium thickness is based on a thorough optimization study.[27] First evaporated chromium films are known to have very high residual stresses,[33–35] which can lead to film cracking and delamination. Our study,[27] using shadow masking, showed that achievable crack-free metallized surfaces of the order of $600 \times 600\ \mu m^2$ can be obtained using a chromium adhesion layer thickness of 5 nm. In contrast, thicker chromium film considerably reduce the achievable crack-free metalized surface, e.g., 10 nm of chromium results in a maximum crack-free metalized surface of $100 \times 100\ \mu m^2$.[27] Regarding thinner films, reducing the chromium film to 2 nm results in film non-uniformity, e.g., some cracking and wrinkling

phenomena appear when a 100 nm thick gold film is added.[27] Indeed, it is well known that metal-insulator percolation transition for very thin evaporated films is about 2 nm for chromium[36] and between 6 nm and 20 nm for gold[37] depending on processing conditions, e.g., vacuum pressure, deposition rate, and substrate temperature.[38] Hence, an optimized chromium/gold bilayer of 5 nm/100 nm has been chosen and thermally evaporated through a specially prepared shadow mask defining a metal mesa array, including $100 \times 100\ \mu m^2$, $300 \times 300\ \mu m^2$, $100 \times 500\ \mu m^2$, and $600 \times 600\ \mu m^2$ square and line shaped metal mesas (see Fig. 1). The deposition rates were 0.2 nm s^{-1} and 0.5 nm s^{-1} for the chromium and the gold, respectively. Note that no *in situ* argon plasma treatment is used for any samples prior to the metal evaporation.

We finally obtain 10:1 PDMS samples (exposed or not to oxygen plasma) metallized with 23 features of width 100 μm, 11 features of width 300 μm, 8 features of width 500 μm, and 7 features of width 600 μm. This allows one to define *filling factors*, i.e., the density of metallization along the sample width direction—see Fig. 1, for each feature dimension, i.e., 0.31, 0.44, 0.53, and 0.56 for the features of widths 100 μm, 300 μm, 500 μm, and 600 μm, respectively. Note that no cracking is observed in the mesas (evaporated onto plasma-exposed PDMS) having a width less than 600 μm. However, we observe cracking in some of the $600 \times 600\ \mu m^2$ features—in agreement with other observations published in Ref. 27 where we report a link between metallization thickness, dimensions, and cracking. Here, following the metallization, some $600 \times 600\ \mu m^2$ features did not contain cracks and were able to be characterized. This can be explained by the fact that for a chromium thickness of 5 nm and a feature width of 600 μm we are very close to the cracking/non-cracking transition[27] and thus highly sensitive to the variations of processing conditions, i.e., deposition rate, thickness, and mask imperfections.

The samples were next subjected to quasi-static mechanical tensile tests using an in-house built sample stretcher allowing both a micrometric translation of the mobile chuck and a simultaneous two probe (Karl Suss probe station) resistance measurement using a Metrix® MX545 multimeter (ITT Corp., USA) of the metallized mesa features. The loading strain was increased by increments of 1.5%, the electrical resistance was measured on the $100 \times 500\ \mu m^2$ metallized mesa features by increments of 6.5% strain, while optical microscope images of 100 μm, 300 μm, 500 μm, and 600 μm width features were taken at key instants. Finally, averaged metallized mesa feature mechanical strains were measured using Digital Image Correlation,[39] allowing us to compare the macroscopic strain loading to the local one.

III. MECHANICAL MODELING

This section presents the mechanical modeling of the metallization/PDMS multi-layer. In order to predict the mechanical behavior of such metal mesa arrays (i.e., Cr/Au—5 nm/100 nm) on a flexible substrate (i.e., plasma-exposed and unexposed PDMS) and understand the parameter set which leads to a significant strain decrease inside the metal mesa—we used a basic mechanical modeling of the metallized multi-layer and the PDMS material[23,27] based on their published elastic mechanical properties.[25,40,41]

First, a reasonable assumption is that the nanometer-thick silica-like layer produced on the 1 mm thick PDMS, by oxygen plasma exposure, only affects the bonding between the metallization and the substrate without affecting the PDMS bulk elastic properties. In addition, due to the very low stiffness (of the order of 100 MPa, Ref. 31) of the silica-like crust, compared to the chromium[40] and the gold[41] one (greater than 100 GPa), it seems reasonable, at least in a first approach, to neglect the silica-like layer in the modeling. Next, we assume a one dimensional model where the PDMS parts (inter-mesa pieces denoted by the subscript "PDMS") and metal mesas (denoted by the subscript "mesa") are in series along the loading direction and where each layer of the metal mesas (denoted by the subscript "l") are in parallel. Finally, we assume that the behavior of each component remains elastic. This last assumption is consistent with the brittle mechanical behavior of thin chromium films[42] and the linear mechanical response observed on gold thin film below $\approx$1% of loading strain[43] as well as on the 10:1 PDMS below $\approx$40% of loading strain.[25] These assumptions allow one to write down the following equations:

$$\begin{cases} \Delta l_{total} &= (n+1)\Delta l_{pdms} + n\Delta l_{mesa} \\ F_{pdms} &= F_{mesa} \\ \varepsilon_{mesa} &= \varepsilon_{mesa}^{l_0} = \cdots = \varepsilon_{mesa}^{l_m} \\ F_{mesa} &= \sum_{l=0}^{m} F_{mesa}^{l} \end{cases}, \tag{1}$$

with $\varepsilon = \frac{\Delta l}{l_0}$ and $\sigma = E\varepsilon = \frac{F}{S}$. The equations above express that, in series, the force is identical in all parts and length variations are cumulated while in parallel this is the opposite. A schematic diagram representing this mechanical model can be seen in Fig. 1.

The deformation ratio between the mean metallized feature strain ε_{mesa} and the macroscopic strain loading ε_{total} can finally be written down as follows:

$$\delta = \frac{\mathbb{S}}{\mathbb{F}(\mathbb{S}-1)+1}, \tag{2}$$

where $\delta = \varepsilon_{mesa}/\varepsilon_{total}$ is the strain ratio, $\mathbb{F} = nd/L$ is the filling factor, and $\mathbb{S} = (e_{pdms}E_{pdms})/(\sum_{l=0}^{m} e_l E_l)$ is the equivalent stiffness ratio. n is the number of mesa, d is the non-deformed mesa length, e_l and E_l are the thickness and the stiffness of the layer l, respectively, and L is the non-deformed gauge section length.

Fig. 2 will be discussed in detail later in the context of the experimental results but an initial brief analysis will allow us to understand the meaning of the figure. First, a filling factor $\mathbb{F}$ equal to unity corresponds to a "blanket" metallization where the metal deposition covers the whole of the PDMS sample surface. Second, an equivalent stiffness ratio $\mathbb{S}$ equal to one corresponds to the case where the metallization rigidity is equal to the substrate rigidity. Values close to these conditions do not allow a reduction of the local strain

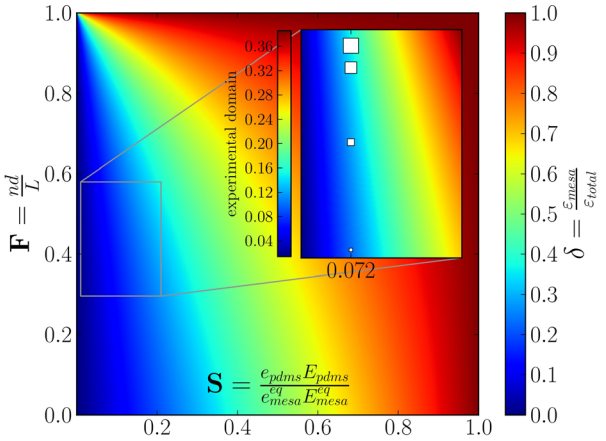

FIG. 2. Mapping of the strain ratio, δ, as a function of the filling factor, $\mathbb{F}$, and the equivalent stiffness ratio, $\mathbb{S}$, for the elastic model of a metal mesa array bonded onto a PDMS substrate. Boxed zone corresponds to the range of filling ratios investigated experimentally ($\mathbb{F} = [0.3 - 0.6]$) and the following strain ratio: $\delta = [0.1–0.21]$, with $E = 2$ MPa for the PDMS. White squares are experimental points positioned using experimental filling factor and strain ratio for the mesa features of widths 100 (smallest), 300, 500, and 600 (biggest) μm.

($\delta \approx 1$)—practically this means that the strain in the metal follows the macroscopic loading strain. In contrast, in order to locally reduce the loading strain to about 90%, the equivalent rigidity of the metallization must be at least ten times higher than the equivalent rigidity of the substrate. Indeed, it can be noted that the model predicts that the parameter $\mathbb{S}$ has a greater effect on the local strain reduction of mesa features than the parameter $\mathbb{F}$. However, the smaller the filling factor, the higher the local strain reduction. Thus, the model also predicts that the density of metallized features, i.e., the system layout, has an important impact on the strain level within each metallized feature. This has been technologically demonstrated and finite element modelled for horseshoe-like stretchable conductors encapsulated in a polymer substrate.[44]

IV. RESULTS AND DISCUSSIONS

Figure 3 presents the mechanical strain and electrical resistance variations as a function of the macroscopic loading strain for the Cr/Au metallized 10:1 PDMS substrates initially exposed to oxygen plasma (see Fig. 3(a)) and for the metallized 10:1 PDMS samples (see Fig. 3(b)), which were not exposed to oxygen plasma.

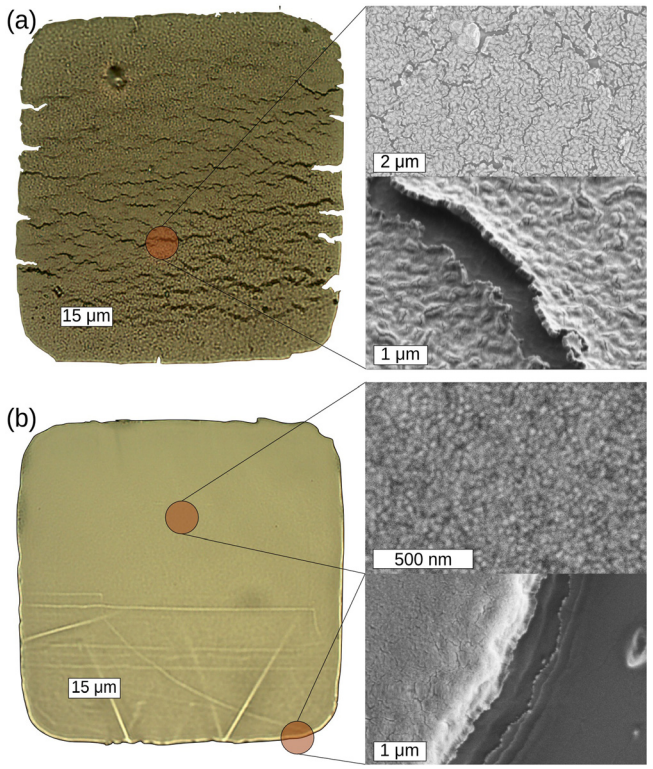

FIG. 4. Optical microscopy images and scanning electron microscopy images of $100 \times 100\,\mu m^2$ thermally evaporated Cr/Au metallized features deposited onto (a) PDMS and (b) oxygen plasma treated PDMS using shadow masking.

Focusing on oxygen plasma exposed samples (see Fig. 3(a)), first, some key points can be noted:

(1) The metallized features deform significantly less than the macroscopic sample. Indeed, we observe, for example, at 10% of loading strain (in the linear domain), a local strain reduction of about 97%, 86%, 85%, and 83% for the Cr/Au mesa features of widths 100 μm ($\mathbb{F} = 0.31$), 300 μm ($\mathbb{F} = 0.44$), 500 μm ($\mathbb{F} = 0.53$), and 600 μm ($\mathbb{F} = 0.56$), respectively. This provides evidence of the influence of the filling factor since, as predicted by the model (see Fig. 2), the smaller the filling factor, the higher is the strain reduction. As stated above, such effects have been partially investigated in specific structures, e.g., horseshoe-like wires,[44] in

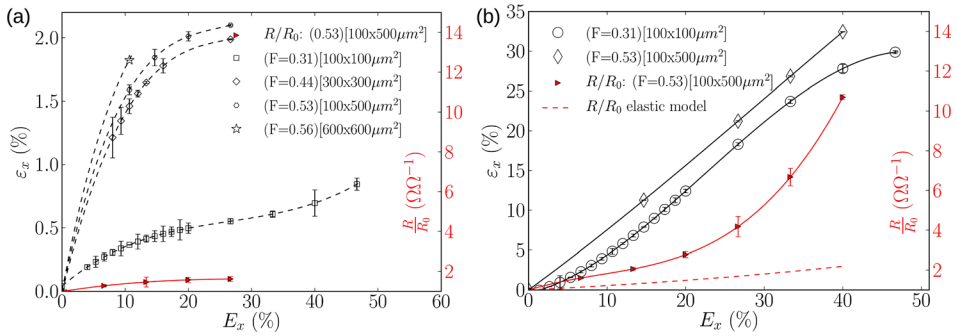

FIG. 3. Evolution of the strain (ε_x) of metallized mesas (Cr/Au—5 nm/100 nm) as a function of the macroscopic loading strain (E_x) for different metallized mesa dimensions: $100 \times 100\,\mu m^2$ ($\mathbb{F} = 0.31$), $300 \times 300\,\mu m^2$ ($\mathbb{F} = 0.44$), $100 \times 500\,\mu m^2$ ($\mathbb{F} = 0.53$), $600 \times 600\,\mu m^2$ ($\mathbb{F} = 0.56$), and evolution of the electrical resistance obtained on $100 \times 500\,\mu$m metallized lines. (a) 10:1 PDMS exposed to 1.5 kJ plasma oxygen at 300 mTorr and (b) 10:1 PDMS samples not exposed to oxygen plasma.

order to understand how the global layout affects the local strain-induced damage. Nevertheless, to our knowledge, no analytical modeling has been provided to predict the strain localization as a function of physical and design parameters.

Experimental points are reported in Fig. 2 taking into account the experimental filling factor of metallized features and the best fit between the experimental and the numerical δ ratios at fixed mechanical properties. First, it allows one to estimate that the experimental equivalent stiffness of the Cr/Au/PDMS regions is about 28 MPa (i.e., 2 MPa/0.072—see Fig. 2)—thus the equivalent stiffness of the Cr(5 nm)/Au(100 nm) metallization is about 245 GPa, which is in very good agreement with thin chromium[40] and gold[41] stiffness values (elastic moduli) found in the literature. Second, this allows a partial validation of the simple analytical model and the predicted sensitivity to the filling factor. Indeed, the model predicts, in relatively good agreement with experiments, a local strain reduction of 90%, 88%, 86%, and 85% for the fill factors 0.31 (100 μm), 0.44 (300 μm), 0.53 (500 μm), and 0.56 (600 μm), respectively. Nevertheless, the very low strain value observed on the features of width 100 μm is underestimated by the model. As we shall see later, it is possible that a uniaxial model (e.g., which does not include Poisson's effect) cannot fully predict all experimental observations.

(2) In agreement with the modeling assumptions (see Fig. 2), one observes: irrespective of the metallized feature dimensions, that the local mean feature strain ε_x evolves in a quasi-linear way as a function of the macroscopic loading strain E_x up to an inflection domain around 1.5%–2%. Knowing that the PDMS has an elastic behavior (at such a strain level), the linearity reflects the elastic behavior of the metallized features below 1.5%–2% of loading strain. Next, the saturation of the mesa feature strain (i.e., implying an increased hardening of the metallizations) is observed before their fracture at $2.0 \pm 0.1\%$, $2.2 \pm 0.1\%$, and $2.2 \pm 0.4\%$ for the features of widths 300 μm, 500 μm, and 600 μm, respectively—almost at the same critical strain, i.e., $\approx$2%. This potentially occurs at different loading strain levels, depending on the filling factor—this seems to be the case for the uncracked features of width 100 μm. It is finally very interesting to note that the observed failure strain value is in total agreement with the failure strain of very thin ($\leq$15 nm) chromium film found in the literature.[42]

(3) The $100 \times 100\ \mu m^2$ features remains un-cracked, due in part to their low filling factor (0.31), up to a loading strain of 47%. Notice that, at such a strain level, the 1 mm thick PDMS substrate actually fractures. Thus, surprisingly, the thick PDMS film fails before the $100 \times 100\ \mu m^2$ metallized features are damaged. This can be explained using the 1st equation of the system 1, which allows one to estimate the mean strain value in the inter-mesa parts (at fracture) to be about 67% with potentially local higher strain concentrations. This is in line with PDMS failure strain level recently reported.[25] Thus, at a specific strain loading, the limited strain within metallized features significantly increase the strain level (here +47%) within the substrate and can damage it.

(4) At the $100 \times 500\ \mu m^2$ metal features fracture point, i.e., at about 30% of loading strain, the electrical resistance is multiplied only by a factor of $\approx$1.63. Notice that the initial resistivity is $20 \times 10^{-8}\ \Omega$ m (not shown here), i.e., about 8 times greater than the bulk gold resistivity ($\rho \approx 2.4 \times 10^{-8}\ \Omega$ m, Ref. 45).

Next, let us focus on the PDMS samples (see Fig. 3(b)), which were not exposed to oxygen plasma prior to Cr/Au metallization. Some key points can also be noted concerning these results:

(1) the experimental strain ratio δ is about 0.71 and 0.81 for the mesa features of widths 100 μm ($\mathbb{F} = 0.31$) and 500 μm ($\mathbb{F} = 0.53$), respectively. Thus, one observes both a slight strain reduction (from macro to micro) and a slight sensitivity to the metallization filling factor. Again, as the analytical model predicts (see Fig. 2), the smaller the filling factor, the higher is the strain reduction. Nevertheless, if we try to estimate the equivalent metallized mesa stiffness required to obtain such strain ratios δ we find, according to Fig. 2, that the Cr(5 nm)/Au(100 nm) metallization deposited onto non-exposed PDMS has an equivalent stiffness of only 10 GPa, i.e., 24.5 times less than the stiffness estimated for oxygen plasma-exposed PDMS substrates. We will see further that this low equivalent modulus actually reflects the fully cracked state of metallized mesas evaporated onto PDMS substrates which have never been exposed to oxygen plasma prior to Cr/Au metallization.

(2) The measured electrical resistance of the $100 \times 500\ \mu m^2$ metal features is multiplied by 10.8 at 40% macroscopic strain loading while the initial resistivity is $76 \times 10^{-8}\ \Omega$ m (not shown here), i.e., 31 times greater than the bulk gold resistivity. In comparison, the geometrical (elastic material: $R/R_0 = (1 + \varepsilon_{total})/(1 - \nu\varepsilon_{total})^2$,[46] ν is the Poisson's ratio) and electrical resistance variation is plotted using dotted line and reaches 2.2 at 40% of loading strain, i.e., of the order of the electrical resistance variation observed on oxygen plasma-exposed PDMS substrate. Thus, while the resistivity of metallized features measured on oxygen plasma-exposed PDMS samples varies only a little and almost linearly, the metallized feature deposited onto the non-exposed PDMS samples varies greatly, indeed quasi-exponentially, as a function of the macroscopic loading strain.

One can thus partially conclude that, by simply exposing the 1 mm thick PDMS substrate to a specific plasma treatment and using an appropriate feature density obtained using a shadow mask, we can produce small metallized features which are able to sustain very high macroscopic strain loadings ($\geq$30%) without significantly deforming ($\leq$2%) and altering their electrical properties, e.g., the initial resistivity ($R_0 \leq 10R_0^{bulk}$) and loading resistivity ($R/R_0 \leq 2$)—as opposed to metallized non-exposed PDMS material. Importantly, this last point implies that metallized features on oxygen plasma exposed PDMS are, in principle, not damaged during such high macroscopic strain values. In addition, the mechanical and electrical behavior of metallized features evaporated onto oxygen plasma-exposed PDMS substrates can be relatively well predicted using basic elastic assumptions and modeling (see Eq. (2)) given above.

Fig. 4 presents optical microscope images and scanning electron microscopy (SEM) images (after mechanical loading) of $100 \times 100\,\mu$m metallized features evaporated on non-exposed PDMS (a) and oxygen plasma treated PDMS (b). Note that the loading direction is vertical. One observes in Fig. 4(a) two types of cracking: some micro-cracks perpendicular to the loading direction, which have appeared during the strain loading and a high density of nano-cracks which appearing following the thermal evaporation metallization—this results in a mottled or "popcorn-like" surface. The lower SEM image allows one to observe that the nano-cracks within metallization also structure the soft PDMS surface. We thus understand here why the equivalent rigidity of such feature is more than twenty times lower than the one expected for a thin Cr/Au film. Indeed, such features actually deform as a combination of small stiff regions (bonded small metal islands) linked by soft parts (i.e., metal delamination). As it was previously described by Graz *et al.*,[47] the electrical continuity is ensured within such a fully cracked metallization by percolation paths through the network of gold film ligaments. This explains why the initial resistivity of such pre-cracked film is much greater than the bulk value and why the electrical resistance versus mechanical strain variation is exponential, i.e., comparable to the increase of the crack density as a function of the loading. Such variations of the resistance can be compatible with some specific applications, e.g., a DC 4-point measurement using a flexible system, and allows a very high strain electrical continuity as demonstrated in Ref. 48. Nevertheless, variations of electrical resistance are certainly incompatible with some applications where the dimensional and electrical properties are required to be constant, e.g., flexible high frequency transmission lines.

In contrast, we observe in Fig. 4(b) that the Cr/Au metal mesa features deposited on oxygen plasma-treated PDMS is crack-free. Inside the features and at the boundaries of the features, the SEM images allow one to observe that the Cr/Au metallized surface is not totally flat but has a slight roughness composed by grains of about 20 nm while the metallization boundaries are delaminated. We suggests that the in-plane high residual stresses in the chromium layer during metallization (≈3 GPa, Ref. 27) leads to a cracking of the silica-like PDMS (SiO_x) layer at the mesa feature boundaries (see Fig. 4(b) bottom zoom) and produces such a nano-crack network observed in the vicinity of the feature boundaries. This reflects both a high cohesion of the metallized features to the oxidized PDMS surface—contrary to that observed in Fig. 4(a), as well as a very strong bonding between the Cr/Au metallization and the silica-like PDMS layer chemically produced on the surface of the PDMS substrate.

Fig. 5 presents the evolution of the metallized mesa feature surface as a function of the loading strain. Fig. 5(a) shows the $100 \times 100\,\mu m^2$ and (b) the $100 \times 500\,\mu m^2$ (where electrical resistance measurement is done). As already discussed above, one observes in Fig. 5(a) that the $100 \times 100\,\mu m^2$ features, evaporated on PDMS not having been exposed to oxygen plasma, deform up to 30% (i.e., $\delta = 0.71$), while the $100 \times 100\,\mu m^2$ features evaporated on oxygen plasma-exposed PDMS deform much less—up to

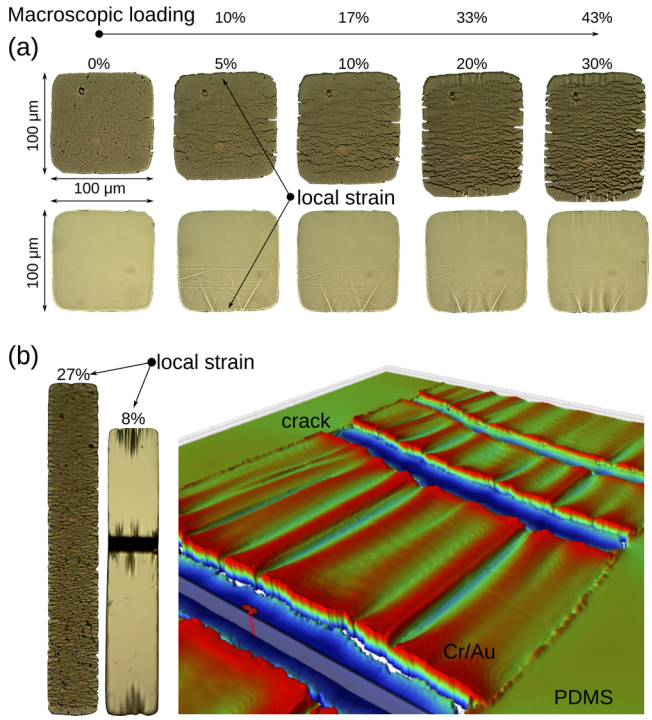

FIG. 5. (a) Optical microscopy images of $100 \times 100\,\mu m^2$ square features at different loading strain instants. (b) Optical microscopy images of $100 \times 500\,\mu m^2$ line feature at 33% of macroscopic loading strain (cracking threshold for the metallized features of width 500 μm deposited on plasma-exposed PDMS using shadow masking). (b) An optical profilometry image of a cracked Cr/Au line deposited onto oxygen plasma-exposed PDMS substrate.

0.8% (i.e., $\delta = 0.017$). The impact of the loading strain on the non-exposed PDMS-based features (see Fig. 5(a)) is crack initiation followed by a progressive increase of the crack density perpendicularly to the loading direction—this leads to the large observed deformation of the feature along this direction. In contrast, the plasma treated PDMS-based features (see Fig. 5(b)) only show a slight (<1%) mechanical longitudinal tension and transversal compression. The latter effect is demonstrated by the early appearance and progressive increase of wrinkles at the upper and lower boundary of the metallized features—caused by the Poisson's effect, i.e., a longitudinal tension-induced lateral compression. Note that in our case this phenomenon is amplified since the transversal filling factor is 0.41 (not shown here) for all features which is higher than the $100 \times 100\,\mu m^2$ axial fill factor ($\mathbb{F} = 0.31$), thus for the $100 \times 100\,\mu m^2$ features the reduction of the macroscopic loading strain is lower transversally than axially.

This last point could potentially explain the difficulty in predicting the low axial strain of $100 \times 100\,\mu m^2$ by using a one dimensional analytic model (see Eq. (2)). Indeed, contrary to the $300 \times 300\,\mu m^2$ ($\mathbb{F} = 0.44$), the $100 \times 500\,\mu m^2$ ($\mathbb{F} = 0.53$), and the $600 \times 600\,\mu m^2$ ($\mathbb{F} = 0.56$) features where the transversal filling factor is lower ($\mathbb{F} = 0.41$), i.e., reduced Poisson's effect, the $100 \times 100\,\mu m^2$ features are clearly subjected to multi-axial loading with a sizable Poisson's effect. Indeed, the local multi-axial loading of a given mesa feature depends on the anisotropy of the filling factor. If the filling factor is isotropic, the ratio of the

longitudinal to transversal strains of the mesa feature depends only on the Poisson's coefficient of the PDMS. In contrast, in the case of an anisotropic filling factor, the local strain behavior (on a particular mesa feature) depends on the size and spacing of the neighboring mesa array. This observation should be investigated in more depth to better understand if the local strain multi-axial nature, i.e., the anisotropy of the filling factor, could enhance the feature strain reduction presented in this work.

Fig. 5(b) shows how metallized features crack on plasma-treated PDMS compared to the cracking mechanism occurring within metallized features deposited onto non-exposed PDMS. The high density of initial nano-cracks within non-exposed PDMS-based metallized lines leads to a high density of micro-cracks at high strain with a quasi-homogenous strain field (not presented here). In contrast, the initial high cohesion and subsequent high bonding of the plasma-treated PDMS-based metallized lines lead to a strain localization—in principle, near to its center—and an abrupt feature cracking when the local critical strain of the feature is reached (≈2% see Fig. 3). At this strain level, the metallized line splits into two undamaged lines and the distance between these parts abruptly increases due to the appearance of a new soft (PDMS) part. A surface profiling analysis of these cracked metallized lines (see Fig. 5—left part) allows one to prove that the cracking leads to the appearance of well-defined new short metallized mesa structures. In addition, we measure a crack depth of about 1.4 μm, i.e., much greater than the expected silica-like PDMS thickness (<40 nm). This suggests a cracking of the silica-like layer as well as in the underlying softer PDMS layer.

V. CONCLUSIONS

An oxygen plasma treatment having a plasma dose of 1.5 kJ (50 W for 30 s) at an oxygen pressure of 300 mTorr allows one to obtain up to $600 \times 600\ \mu m^2$ crack-free Cr/Au (5 nm/100 nm) metallized features on highly flexible (10:1) 1 mm thick PDMS substrates. For such metallized features, we observe an in-feature strain reduction of about 90% depending on the equivalent stiffness ratio and metallization surface filling factor, i.e., the metallization pattern density/layout. We also observe that the smaller the equivalent stiffness ratio and filling factor, the higher is the strain reduction. The mechanical behavior of the multi-layer can be successfully predicted using a one dimensional analytical model; and slight deviations of the experimental observations and the modeling suggest a positive impact of the metallization filling factor anisotropy. Finally, the electrical resistance of oxygen plasma-exposed PDMS-based metallized $100 \times 500\ \mu m^2$ lines is around eight times higher than the calculated bulk gold resistance but remains stable ($R/R_0 < 2$) while the macroscopic strain loading reaches 30%. The analysis of the connection between polymer surface treatments, metallization density, and/or mesa feature dimensions on a soft substrate provides key information concerning top-down metallization for flexible electronics, i.e., metallizing without having to employ complicated transfer and bonding methods from rigid to soft substrate (bottom-up). The findings will be useful for designers of flexible radio frequency transmission line technology and soft metamaterials. Finally, it would be interesting in a near future to analyse how constraints associated to direct soft material metallization, e.g., critical crack-free surfaces,[27] and constraints associated with the system design, e.g., the local strain dependence on the global layout/architecture, can be taking into account for the design of stretchable interconnections.

ACKNOWLEDGMENTS

The work was performed within the Laser Processing Platform for Multifunctional Electronics on Flex (LEAF—ANR-11-EQPX-0025) EQUIPEX project—funded by the French Government. The authors thank Dr. Emmanuel Dubois (Head of the LEAF project) for the use of equipment purchased within the project. This work was also partly supported by the French RENATECH network.

[1]A. Nathan, A. Ahnood, M. T. Cole, S. Lee, Y. Suzuki, P. Hiralal, F. Bonaccorso, T. Hasan, L. Garcia-Gancedo, A. Dyadyusha *et al.*, Proc. IEEE **100**, 1486 (2012).
[2]S. Mack, M. Meitl, A. Baca, Z.-T. Zhu, and J. Rogers, Appl. Phys. Lett. **88**, 213101 (2006).
[3]Y. Sun and J. A. Rogers, Adv. Mater. **19**, 1897 (2007).
[4]F. N. Ishikawa, H.-k. Chang, K. Ryu, P.-c. Chen, A. Badmaev, L. Gomez De Arco, G. Shen, and C. Zhou, ACS Nano **3**, 73 (2008).
[5]J. A. Rogers, D.-Y. Khang, Y. Sun *et al.*, "Stretchable form of single crystal silicon for high performance electronics on rubber substrates," U.S. patent 8,198,621 (12 June 2012).
[6]D. S. Gray, J. Tien, and C. S. Chen, Adv. Mater. **16**, 393 (2004).
[7]T. Li, Z. Suo, S. P. Lacour, and S. Wagner, J. Mater. Res. **20**, 3274 (2005).
[8]H. C. Ko, M. P. Stoykovich, J. Song, V. Malyarchuk, W. M. Choi, C.-J. Yu, J. B. Geddes Iii, J. Xiao, S. Wang, Y. Huang *et al.*, Nature **454**, 748 (2008).
[9]D. Cotton, A. Popel, I. Graz, and S. Lacour, J. Appl. Phys. **109**, 054905 (2011).
[10]I. M. Graz, D. P. Cotton, A. Robinson, and S. P. Lacour, Appl. Phys. Lett. **98**, 124101 (2011).
[11]A. Romeo, Q. Liu, Z. Suo, and S. Lacour, Appl. Phys. Lett. **102**, 131904 (2013).
[12]R. Seghir and S. Arscott, "Photo-hardenable and patternable PDMS/SU-8 hybrid functional material: A smart substrate for flexible systems," J. Polym. Sci. B: Polym. Phys. (published online).
[13]H.-J. Kim, C. Son, and B. Ziaie, Appl. Phys. Lett. **92**, 011904 (2008).
[14]G. Gustafsson, Y. Cao, G. Treacy, F. Klavetter, N. Colaneri, and A. Heeger, Nature **357**, 477 (1992).
[15]J. M. Woo, D. Kim, S. Hussain, and J.-H. Jang, Opt. Express **22**, 2289 (2014).
[16]S. Walia, C. M. Shah, P. Gutruf, H. Nili, D. R. Chowdhury, W. Withayachumnankul, M. Bhaskaran, and S. Sriram, Appl. Phys. Rev. **2**, 011303 (2015).
[17]J. Li, C. M. Shah, W. Withayachumnankul, B. S.-Y. Ung, A. Mitchell, S. Sriram, M. Bhaskaran, S. Chang, and D. Abbott, Appl. Phys. Lett. **102**, 121101 (2013).
[18]D. Morits, M. Morits, V. Ovchinnikov, M. Omelyanovich, A. Tamminen, S. Tretyakov, and C. Simovski, J. Opt. **16**, 032001 (2014).
[19]G. Li, S. Chen, W. Wong, E. Pun, and K. Cheah, Opt. Express **20**, 397 (2012).
[20]I. M. Pryce, K. Aydin, Y. A. Kelaita, R. M. Briggs, and H. A. Atwater, Nano Lett. **10**, 4222 (2010).
[21]S. Aksu, M. Huang, A. Artar, A. A. Yanik, S. Selvarasah, M. R. Dokmeci, and H. Altug, Adv. Mater. **23**, 4422 (2011).
[22]J. Li, C. M. Shah, W. Withayachumnankul, B. S.-Y. Ung, A. Mitchell, S. Sriram, M. Bhaskaran, S. Chang, and D. Abbott, Opt. Lett. **38**, 2104 (2013).
[23]S. P. Lacour, S. Wagner, R. J. Narayan, T. Li, and Z. Suo, J. Appl. Phys. **100**, 014913 (2006).
[24]C. Yu, Z. Wang, H. Yu, and H. Jiang, Appl. Phys. Lett. **95**, 141912 (2009).

[25]R. Seghir and S. Arscott, Sens. Actuators, A **230**, 33 (2015).
[26]D. Corning, "Sylgard® 184 silicone elastomer kit web page," http://www.dowcorning.com/applications/search/products/Details.aspx?prod=01064291.
[27]R. Seghir and S. Arscott, "Controlled mud-crack patterning and self-organized cracking of polydimethylsiloxane elastomer surfaces," Sci. Rep. (submitted).
[28]S. Béfahy, P. Lipnik, T. Pardoen, C. Nascimento, B. Patris, P. Bertrand, and S. Yunus, Langmuir **26**, 3372 (2009).
[29]F. A. Bayley, J. L. Liao, P. N. Stavrinou, A. Chiche, and J. T. Cabral, Soft Matter **10**, 1155 (2014).
[30]P. Goerrn and S. Wagner, J. Appl. Phys. **108**, 093522 (2010).
[31]Y. Yang, K. Kulangara, R. T. Lam, R. Dharmawan, and K. W. Leong, ACS Nano **6**, 8591 (2012).
[32]O. Akogwu, D. Kwabi, A. Munhutu, T. Tong, and W. Soboyejo, J. Appl. Phys. **108**, 123509 (2010).
[33]R. Berger and H. Pulker, in *International Technical Conference/Europe* (International Society for Optics and Photonics, 1983), pp. 69–73.
[34]G. Janssen and J.-D. Kamminga, Appl. Phys. Lett. **85**, 3086 (2004).
[35]M. Cordill, A. Taylor, J. Schalko, and G. Dehm, Metall. Mater. Trans. A **41**, 870 (2010).
[36]J. Lourens, S. Arajs, H. Helbig, E.-S. A. Mehanna, and L. Cheriet, Phys. Rev. B **37**, 5423 (1988).
[37]M. Walther, D. Cooke, C. Sherstan, M. Hajar, M. Freeman, and F. Hegmann, Phys. Rev. B **76**, 125408 (2007).
[38]N. Kaiser, Appl. Opt. **41**, 3053 (2002).
[39]R. Seghir, J.-F. Witz, and S. Courdert, "Yadics—Digital image correlation 2/3d software," http://www.yadics.univ-lille1.fr.
[40]R. Whiting and M. Angadi, Meas. Sci. Technol. **1**, 662 (1990).
[41]F. Avilés, L. Llanes, and A. Oliva, J. Mater. Sci. **44**, 2590 (2009).
[42]H. Jin, W.-Y. Lu, M. Cordill, and K. Schmidegg, Exp. Mech. **51**, 219 (2011).
[43]R. Emery and G. Povirk, Acta Mater. **51**, 2079 (2003).
[44]Y.-Y. Hsu, M. Gonzalez, F. Bossuyt, F. Axisa, J. Vanfleteren, and I. De Wolf, J. Micromech. Microeng. **20**, 075036 (2010).
[45]W. M. Haynes, *CRC Handbook of Chemistry and Physics* (CRC Press, 2013).
[46]P. Mandlik, S. P. Lacour, J. W. Li, S. Y. Chou, and S. Wagner, IEEE Electron Device Lett. **27**, 650 (2006).
[47]I. M. Graz, D. P. J. Cotton, and S. P. Lacour, Appl. Phys. Lett. **94**, 071902 (2009).
[48]S. Wagner, S. P. Lacour, J. Jones, I. H. Pai-hui, J. C. Sturm, T. Li, and Z. Suo, Physica E: Low-Dimen. Syst. Nanostruct. **25**, 326 (2004).